ELSEVIER

Journal of Alloys and Compounds 446–447 (2007) 280–289

Journal of ALLOYS AND COMPOUNDS

www.elsevier.com/locate/jallcom

Thermal decomposition of AlH_3 studied by *in situ* synchrotron X-ray diffraction and thermal desorption spectroscopy

J.P. Maehlen [a], V.A. Yartys [a,*], R.V. Denys [a,b], M. Fichtner [c], Ch. Frommen [c], B.M. Bulychev [d], P. Pattison [e], H. Emerich [e], Y.E. Filinchuk [e], D. Chernyshov [e]

[a] *Institute for Energy Technology, P.O. Box 40, Kjeller No-2027, Norway*
[b] *Physico-Mechanical Institute of the National Academy of Science of Ukraine, 5, Naukova Str., 79601 Lviv, Ukraine*
[c] *Institute of Nanotechnology, Forschungszentrum Karlsruhe GmbH, P.O. Box 30640, D-76021 Karlsruhe, Germany*
[d] *Chemistry Department, Moscow State University, Leninskie Gori, Moscow 119992, MSU, Chemistry Department, Russia*
[e] *Swiss-Norwegian Beam Line, ESRF, BP 220, F-38043 Grenoble, France*

Received 30 October 2006; received in revised form 28 November 2006; accepted 29 November 2006
Available online 12 January 2007

Abstract

The thermal decomposition of alane was investigated by application of synchrotron X-ray diffraction (SR-XRD) and thermal desorption spectroscopy (TDS). Two polymorphs were studied, α- and γ-AlH_3. Activation energies, anisotropic volume expansions, and phase transformation paths were found. In addition, the crystal structure data, including structure of hydrogen sublattice, and small charge transfer from the aluminium towards the hydrogen sites were observed during a high-resolution SR-XRD study of α-AlH_3.

Keywords: Hydrogen absorbing materials; Crystal structure; Phase transitions; Synchrotron radiation

1. Introduction

To utilize renewable energy sources, hydrogen and electricity are considered as an ideal combination of energy carriers, providing versatile and environmentally benign solutions. Every step in a complete hydrogen energy cycle, which includes hydrogen production from water by electrolysis, hydrogen storage and conversion into electricity in the fuel cell stack, needs to be sufficiently improved to increase the competitiveness of hydrogen energy with the available energy systems. Hydrogen storage is considered as the most important issue to be solved. An efficient hydrogen storage solution should combine several key features including high hydrogen storage densities, volumetric and gravimetric, fast and easy reversible H loading/H release, together with affordable price and fulfilment of the safety requirements. A storage system satisfying all these beneficial features, unfortunately, is not developed yet. Even though solid state storage materials, first of all reversible metal hydrides, have been appreciated as an efficient way for reaching high volumetric efficiency of the storage system and fast rates of hydrogen exchange, reaching these advantages has always been paid by a price of having a rather poor gravimetric hydrogen storage capacity.

To reach the high gravimetric hydrogen densities required for commercially competitive hydrogen storage solutions for the transport sector, metal hydride systems containing light elements are needed. In the present work we have focused our studies on the binary metal-hydrogen system of such a type, namely on the aluminium trihydride (alane). Aluminium trihydride alane is considered as a prospective solid H storage material, having high gravimetric (10 wt.% H) and volumetric density of H (2 times higher compared to LH_2) and, also, because of its convenient range of thermal stability. AlH_3 forms several polymorphic modifications, which are often polymers $(AlH_3)_n$ [1]. α-Alane AlH_3 was first synthesized in 1947 by an exchange reaction between $AlCl_3$ and lithium hydride in ether solution [2]. This binary hydride has a covalent Al–H bonding and exhibits dielectric properties. α-AlH_3, the most stable modification of alane, has a trigonal crystal structure (space group $R\bar{3}c$) [3,4] and is composed of the corner-sharing AlH_6 octahedra. The AlH_6 octahedra remain as the building elements of the crystal struc-

* Corresponding author. Tel.: +47 63 80 64 53; fax: +47 63 81 29 05.
E-mail address: volodymyr.yartys@ife.no (V.A. Yartys).

0925-8388/$ – see front matter © 2006 Elsevier B.V. All rights reserved.
doi:10.1016/j.jallcom.2006.11.199

tures of the other polymorphs of AlH_3. However, their packing densities decrease compared to α-AlH_3. This decrease is due to the formation of cavities in γ-AlH_3 [5] or from the large empty channels in between the octahedra in β-AlD_3 [6]. The double bridge Al–2 H–Al bonds were firstly experimentally observed for the Al-based hydrides [5] in γ-AlH_3 containing the edge-sharing AlH_6 octahedral units. NMR investigation of the γ-AlH_3 [7] showed formation of distorted coordination polyhedra of H around Al, in agreement with the data of the crystal structure studies [5].

Metastable alane does not release hydrogen at normal conditions and is stable in air, probably due to the formation of oxide layers at the surface. At atmospheric pressure AlH_3 desorbs hydrogen at rather moderate temperatures (350–400 K, depending on its preparation history). Achieving sufficiently rapid and controllable decomposition of AlH_3 and proposal for efficient synthesis routes to make the system Al–AlH_3 reversible are focused in ongoing research (see, e.g. [8–11]). Thermodynamic characterisation of the polymorphs of alane and studies of the kinetics of hydrogen release facilitated by alkali metal hydrides showed that during decomposition β- and γ-AlH_3 transform into the alpha modification and that significantly fast hydrogen release from alane starts at the temperatures well below 100 °C. However, detailed mechanism of the decomposition process and its kinetics at different temperatures requires further investigation in order to propose the most optimal way of utilizing AlH_3-based systems for hydrogen supply aimed for the use in automotive mobile applications.

This work was focused on studies of the thermal decomposition of alane by application of synchrotron X-ray diffraction (SR-XRD) and thermal desorption spectroscopy (TDS). Two polymorphs were studied, α- and γ-AlH_3.

2. Experimental details

Samples from three different alane batches were investigated in this work; two α-AlH_3 batches (aged α-AlH_3 and fresh α-AlH_3), and one γ-AlH_3. Several methods for the wet chemical synthesis of AlH_3 have been reported in the literature decades ago. The most difficult problem is to obtain AlH_3 free of solvent without decomposing the sample [1,2] as temperatures of solvent desorption and hydride decomposition are close to each other. Both α-AlH_3 samples were prepared using modifications of a method described by Brower et al. [1]. Preparation method of the γ-AlH_3 modification is described in [5]. All samples were stored under argon atmosphere, in airtight containers for the time between the synthesis and the measurements.

Temperature desorption spectroscopy (TDS) study of the hydrogen release from the samples were performed by heating a small amount of the selected sample (less than 100 mg) in a stainless steel autoclave at a constant heating

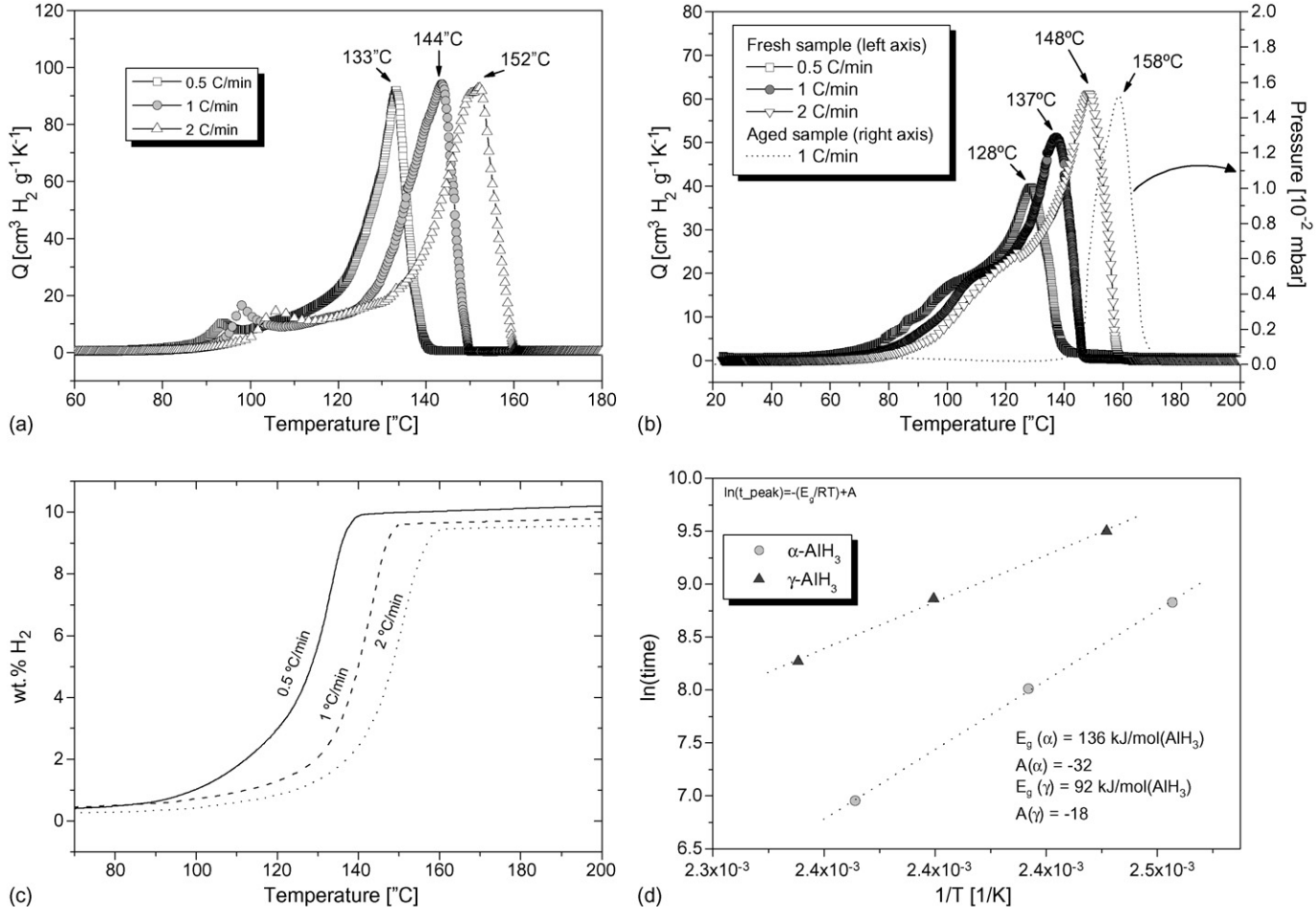

Fig. 1. Thermal desorption spectra of hydrogen desorption from AlH_3, (a) γ-AlH_3; (b) fresh and aged α-AlH_3; note that the aged sample shows higher desorption temperatures with more symmetric peak shape; probably due to thicker and more evenly distributed oxide layers; (c) integrated desorption traces for γ-AlH_3; (d) Arrhenius plots for α- and γ-AlH_3. The activation energy for the γ is lower than for the α.

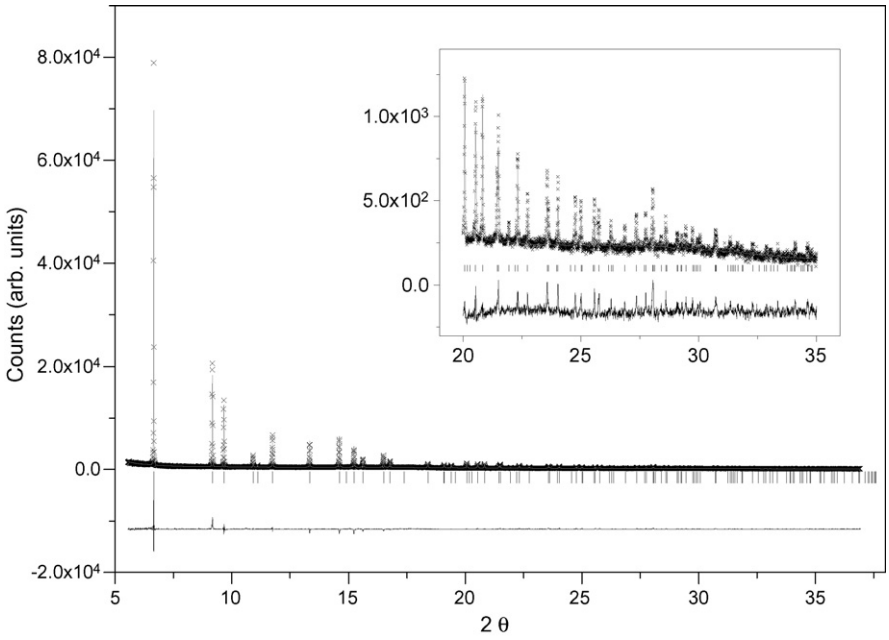

Fig. 2. Rietveld-type plots of the SR-XRD pattern for α-AlH_3 (λ = 0.37504 Å) collected at room temperature showing observed (crosses), calculated (upper line) and difference (bottom line) plots. The positions of the Bragg peaks are shown as ticks. An enlargement of the high-angle part is shown in the inset.

rate. Dynamic secondary vacuum in the measurements setup was maintained by using a turbo-molecular pumping system, while desorption pressure was continuously monitored by the vacuum sensor.

SR-XRD studies of AlH_3 were performed at the Swiss-Norwegian Beam Lines (SNBL) at the European Synchrotron Radiation Facility (ESRF), Grenoble, France. Three different experiments were performed:

1. High-resolution scan at room temperature of the aged α-AlH_3 sample (station BM01B).
2. *In situ* scan of the aged α-AlH_3 sample (station BM01B), heating rate 1 K/min.
3. *In situ* scan of the γ-AlH_3 sample (station BM01A), heating rate 1/2 K/min.

The *in situ* measurements were performed using a setup designed for *in situ* studies of the chemical processes occurring in hydrogen or gas/vacuum atmosphere [12–14]. In this setup, a small amount of the sample is put in a 0.7 mm quartz glass capillary filling approximately 1–2 mm of the capillary's bottom part. The capillary is hermetically connected to the gas system using a carbon ferrule mounted in a T-piece, which, in turn, is attached to the goniometer head. Averaging over the different orientations of the crystallites, resulting in the elimination of preferred orientation effects in the collected diffraction data, is achieved by oscillating the setup around the axis of the capillary. The required elasticity of the setup is made possible by using a flexible PEEK polymer tubing connection between the microreaction cell and the flow system. Vacuum is created using a turbo molecular vacuum pump. Except for the PEEK tubing allowing the oscillation of the sample cell, stainless steel tubes are used for the connections to prevent oxygen diffusion through the tubes during the experiments.

The diffractometer at station BM01B (Si(1 1 1) channel-cut monochromator, scintillation detectors) is equipped with six counting chains, with an angular offset in 2θ of ∼1.1°. For *in situ* measurements, in order to keep the counting time per scan as low as possible, the detector bank is moved by 1.2° during one measurement and the data from the six different detectors are added using a data-binning program. One data set (2θ = 6.07–12.67°) was collected in 2 min during the heating of the sample under secondary vacuum conditions. The high-resolution measurement of the aged α-AlH_3 was performed in steps of 0.005°

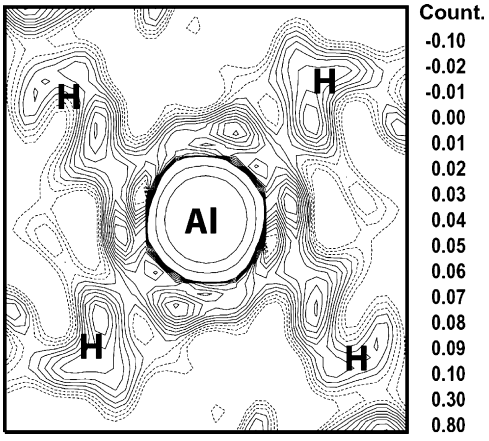

Fig. 3. Fourier transform of the observed SR-XRD pattern (GSAS Rietveld refinements) showing the Al–H bonds (equatorial plane of the octahedron containing 4 H atoms is selected).

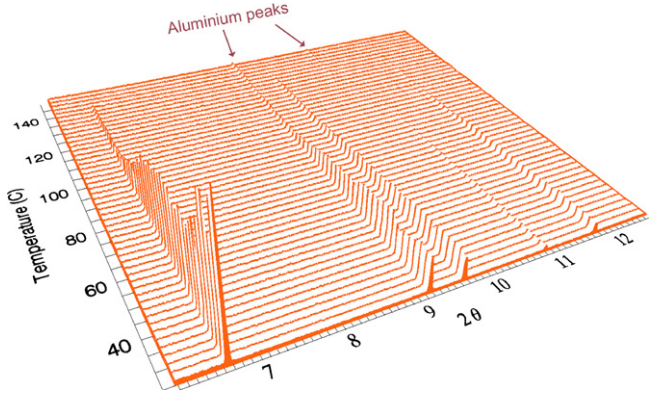

Fig. 4. *In situ* SR-XRD pattern of the thermal decomposition of α-AlH_3 (heating rate 1 °C/min). The α-AlH_3 peaks are diminishing during the heating, indicating amorphisation. At higher temperatures small aluminium peaks appear indicating a nucleation and growth process for the aluminium formation.

in the 2θ range from 5.540° to 36.935°. A wavelength of 0.37504(2) Å was used in both experiments.

Experimental data at BM01A were collected using a MAR2300 image plate detector and then integrated using the software Fit2D. The wavelength ($\lambda = 0.71118$ Å) and sample to detector distance ($d = 199.768$ mm, giving a usable 2θ range of about 1–40° for the 1D patterns) were calibrated from an individual run of a LaB_6.

All powder diffraction data were analysed by the Rietveld whole-profile refinement method [15] using the General Structure Analysis System (GSAS) software [16]. Peak shapes were described by a multi-term Simpson's rule integration of the pseudo-Voigt function [17,18], which includes the asymmetry correction according to Finger et al. [19]. Anisotropic line broadening of the diffraction pattern was observed for the γ-polymorph and was accounted for by refinements using the Thompson–Cox–Hastings pseudo-Voigt type function as proposed in [20].

3. Results and discussion

3.1. Thermal desorption spectroscopy

Fresh α-, and γ-AlH_3 samples were studied by TDS at three different constant heating rates ($\Delta T = 0.5$, 1, and 2 K/min). A two-peak desorption behaviour was observed for all runs (see Fig. 1a and b). Prior to the main desorption peak which appeared at around 130–160 °C, a smaller, low temperature desorption event was observed. It is well pronounced as a separate desorption peak in case γ-AlH_3 (Fig. 1a) and seen as a shoulder on a low-temperature side of the peak observed for the α-AlH_3 (Fig. 1b). For γ-AlH_3 it is reasonable to suggest that the low-temperature event corresponds to a direct decomposition process γ-$AlH_3 \rightarrow Al + 3/2\ H_2$; the second, main event, is associated with a decomposition of α-AlH_3, which is formed first during the heating of γ-AlH_3. In case of α-AlH_3, since hydrogen release from this modification should be a single step process, it is likely that the observed behaviour is due to non-uniform surface properties of the different parts of the sample because of the variations in the covering by the particles protective oxide layer.

Activation energies for the desorption process from AlH_3 were found from Arrhenius plots: $E_a = 136$ and 92 kJ/mol AlH_3, for α-AlH_3 and γ-AlH_3, respectively. Graetz and Reilly reported that the activation energy might vary with the age of the sample. They found between 102 and 150 kJ/mol for the α-phase [10].

A TDS run of the aged α-AlH_3 sample was also performed. Compared to fresh samples of α-AlH_3, a much higher desorption temperature was observed for the aged sample. Experimental data and the Arrhenius plots of the TDS experiments are presented in Fig. 1.

3.2. High-resolution SR-XRD investigation of α-AlH_3

The high-resolution SR-XRD pattern of α-AlH_3 was indexed in trigonal setting, space group $R\bar{3}c$ (No. 167). The refinements yielded unit cell parameters: $a = 4.44994(5)$ Å; $c = 11.8200(2)$ Å, and $V = 202.701(4)$ Å^3 which agree well with the reference data: $a = 4.449$ Å; $c = 11.804$ Å; $V = 202.34$ Å^3 [3]. Since Al has a relatively low atomic number, it was possible to locate the hydrogen sublattice during the refinements, starting with Al placed in a special position 6*a* [0, 0, 0] and performing difference Fourier analysis. Performing the refinements without including the H position gave the following best goodness-of-fit parameters: $R_{wp} = 14.2\%$, $R_p = 11.7\%$, and $\chi^2 = 6.0$. Including the hydrogen atom (at site 18*e* [0.625(2), 0, 1/4]), the quality of the fit significantly improved, giving goodness-of-fit parameters of $R_{wp} = 12.1\%$, $R_p = 10.6\%$, and $\chi^2 = 4.9$. Fig. 2 shows the Rietveld-type plots of the high-resolution data.

The refinements yielded an Al–H bonding distance of 1.712(3) Å and an octahedral coordination of Al into AlH_6 units where bridge bonds Al–H–Al are formed with a bond angle of 141°. Furthermore, they indicated a small charge transfer from Al to H corresponding to the formation of $Al^{+0.15}$ and $H^{-0.05}$. This charge distribution can be observed in the Fourier transform of the observed XRD pattern as shown in Fig. 3. We note a good

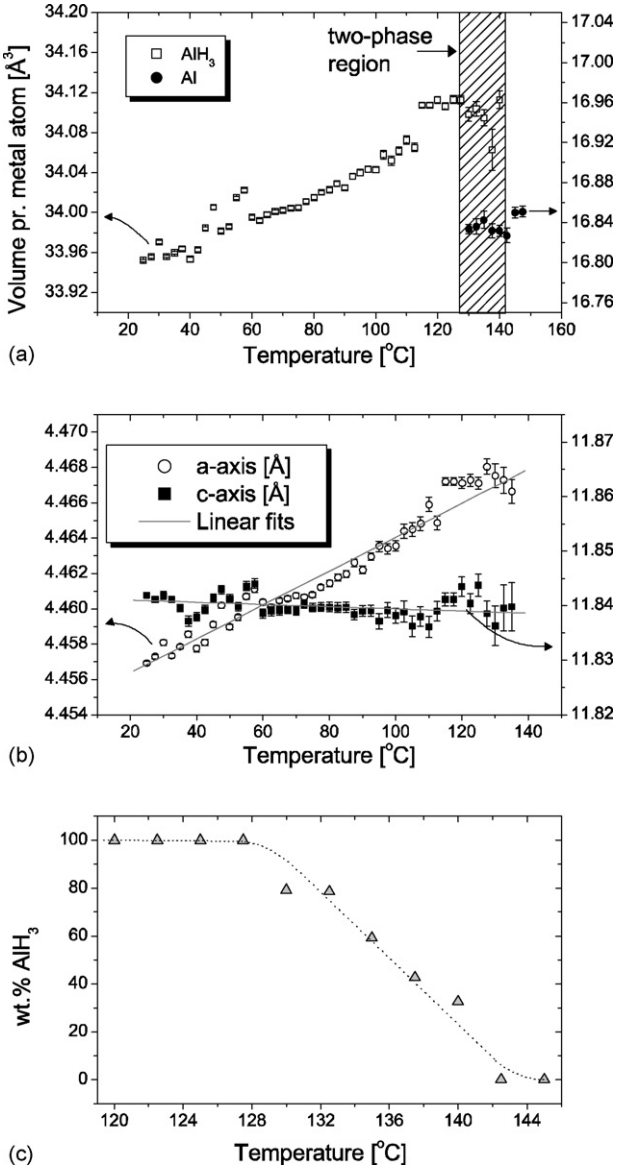

Fig. 5. Results from the refinements of the *in situ* SR-XRD patterns of the aged α-AlH_3 thermal decomposition *vs.* temperature; (a) volumes of the unit cells of the crystal structures of alane and Al metal (per one mole AlH_3/Al), (b) evolution of the unit cell parameters of the hydride during the heating, and (c) temperature-dependent fraction of the crystalline aluminium hydride (by mass) in the system (the refinements included crystalline aluminium and crystalline aluminium hydride).

correspondence between the data of the present powder XRD work and the results of the powder neutron diffraction study of AlD_3 [3], where an Al–D bond distance of 1.715 Å in the AlD_6 octahedra was reported.

Hydrogenation is accompanied by a volume increase of 103.5 (!)% equivalent to 5.73 Å^3/atom H. We note that these numbers are significantly higher compared to the conventional metal/intermetallic hydrides where both corresponding values are significantly lower, respectively, 20–30% and 2.5–3.0 Å^3/atom H [21,22]. This dramatic increase of the unit cell volume is accompanied with an enlargement of the closest Al–Al distances of 13.3% (growing from 2.86 Å in the alloy to 3.24 Å in the hydride).

3.3. *In situ* SR-XRD investigation of the α-AlH_3 to Al transformation

The *in situ* diffraction pattern of the decomposition of the hydride were collected in the temperature range 25–150 °C (see Fig. 4). Rietveld-type refinements of the data were performed (goodness-of-fit parameters for the refinements were all rather large, with R_{wp} in the range 13–28%) and showed that on heating a linear increase of the unit cell dimensions of AlH_3 takes place in an interval from RT to ∼125 °C (a = 4.46; c = 11.83 Å for T = 135 °C; see Fig. 5a and b). The volume expansion is pronouncedly anisotropic, as can be seen from Fig. 5b. Indeed, the c-axis is almost constant in the temperature interval 25–125 °C ($\Delta c/c \sim -0.02\%$). This contrasts to a significant expansion along [1 0 0]: $\Delta a/a \sim 0.28\%$. The latter expansion can mainly be attributed to the elongations of the bridge bonds Al–H–Al aligned along [1 $\bar{1}$ 1/2], which are expanding from 3.243 to 3.248 Å ($\Delta d/d \sim 0.17\%$).

During the heating, a continuous decrease of the intensities of the pattern of AlH_3 was observed indicating a gradual decomposition of the crystalline hydride phase, probably forming amorphous aluminium. This decrease was not accompanied by any significant broadening of the peaks. The intensities of the diffraction peaks from Al firstly appeared at ∼135 °C and then

Table 1
Selected parameters derived from Rietveld-type refinements of the *in situ* SR-XRD data of the thermal decomposition of AlH_3

Parameters						
In situ SR-XRD study of thermal decomposition of 'aged' α-AlH_3						
T (°C)[a]	30	80	100	115	127.5	137.5
α-AlH_3[b]						
a (Å)	4.4581(1)	4.4614(2)	4.4636(3)	4.4672(2)	4.4681(4)	4.468(2)
c (Å)	11.8420(7)	11.8497(9)	11.838(1)	11.841(1)	11.839(2)	11.82(1)
V (Å^3)	203.82(1)	204.09(1)	204.26(2)	204.64(1)	204.64(3)	204.4(1)
v (Å^3)[c]	33.970(2)	34.015(2)	34.043(3)	34.107(2)	34.113(4)	34.06(2)
wt.%	100	100	100	100	100	42.6
No. var.[d]	14	13	10	10	10	13
R_{wp} (%)	17.68	16.61	18.17	18.87	17.22	16.26
In situ SR-XRD study of thermal decomposition of γ-AlH_3						
T (°C)[a]	30	80	88	95	100	115
α-AlH_3[b]						
a (Å)	4.4438(3)	4.4493(3)	4.4524(1)	4.4530(1)	4.4534(1)	4.4525(6)
c (Å)	11.807(1)	11.810(1)	11.8110(6)	11.8111(4)	11.8110(5)	11.809(3)
V (Å^3)	201.92(3)	202.48(2)	202.77(1)	202.829(7)	202.858(8)	202.75(5)
v (Å^3)[c]	33.653(4)	33.746(4)	33.796(2)	33.805(1)	33.810(1)	33.791(8)
wt.%	15.97	16.354	32.49	44.00	38.91	6.65
γ-AlH_3[e]						
a (Å)	5.3762(4)	5.3757(6)	5.3758(5)	5.376(1)	5.375(4)	–
b (Å)	7.3431(6)	7.3447(7)	7.3450(8)	7.344(2)	7.343(7)	–
c (Å)	5.7684(3)	5.7708(4)	5.7711(4)	5.7707(8)	5.771(4)	–
V (Å^3)	227.72(2)	227.85(3)	227.87(3)	227.82(6)	227.8(2)	–
v (Å^3)[c]	37.954(4)	37.975(4)	37.979(5)	37.97(1)	37.97(4)	–
wt.%	70.62	68.83	50.56	19.50	3.32	<0.5
x_2	0.7886(5)	0.7882(6)	0.7873(7)	0.785(1)	0.725(8)	–
y_2	0.0830(4)	0.0831(5)	0.0829(6)	0.082(1)	0.087(6)	–
No. var.[d]	37	37	37	37	34	26
R_{wp} (%)	4.26	4.25	3.79	3.76	3.82	4.4

Standard deviations are given in parentheses.

[a] Estimated error in temperature is ∼±5 °C.

[b] Crystal structure data for α-AlH_3. Space group $R\bar{3}c$; 6 Al in 6*a* (0, 0, 0); 18 H in 18*e* (0.63, 0, 0).

[c] Molar volume (unit cell volume/6 f.u. AlH_3).

[d] No. of variables refined in the Rietveld-type refinements.

[e] Crystal structure data for γ-AlH_3 [5]. Space group *Pnnm*; 2 Al1 in 2*b* (0, 0, 1/2); 4 Al2 in 4*g* (x_2, y_2, 0); 2 H1 in 2*d* (0, 1/2, 1/2); 4 H2 in 4*g* (0.16, 0.24, 1/2); 4 H3 in 4*g* (0.43, 0.64, 1/2); 8 H4 in 8*h* (0.79, 0.08, 0.30).

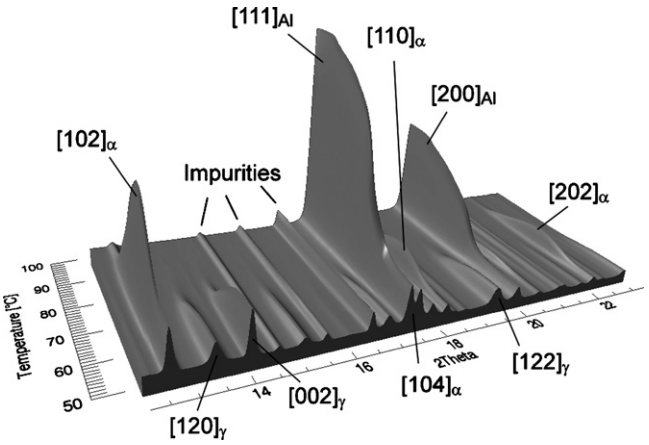

Fig. 6. *In situ* SR-XRD pattern of γ-AlH_3 thermal decomposition (in the temperature range 50–100 °C, heating rate 1/2 °C/min). The γ-AlH_3 peaks observed in the low temperature region diminish as α-AlH_3 starts to form. At higher temperatures, a relatively fast growth of the aluminium diffraction peaks is observed.

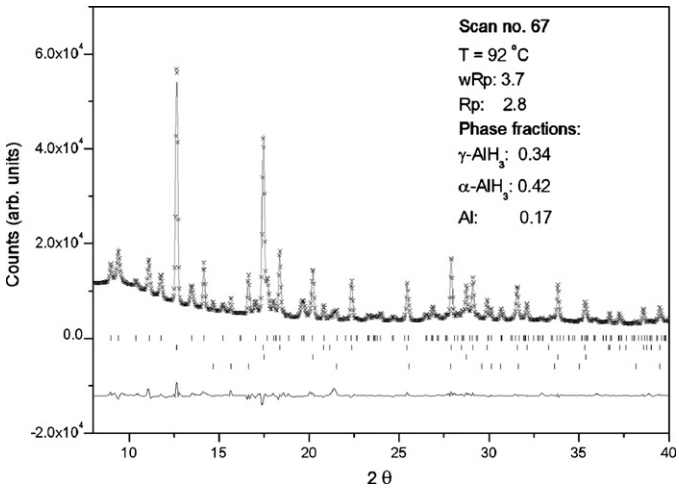

Fig. 7. Rietveld-type plots of the γ-AlH_3 sample from the *in situ* scan (λ = 0.71118 Å) collected at 92 °C showing observed (crosses), calculated (upper line) and difference (bottom line) plots. The positions of the Bragg peaks are shown as ticks (from top to bottom: γ-AlH_3, α-AlH_3, Al).

gradually increased with raising temperature. At $T \sim 145$ °C, the hydride peaks completely vanished indicating completeness of the transformation $AlH_3 \rightarrow Al$. The fraction of the hydride observed in the SR-XRD patterns as a function of the temperature is given in Fig. 5c. These *in situ* data agree well with the TDS measurements showing the onset of the peak of H desorption at ∼140 °C as can be seen in Fig. 1b. Crystallographic and Rietveld refinement parameters for selected scans are presented in Table 1.

3.4. *In situ* SR-XRD investigation of the thermal decomposition of γ-AlH_3

The initial sample used in the *in situ* SR-XRD experiment contained mainly γ-AlH_3 with minor additions of α-AlH_3 and aluminium. Goodness-of-fit parameters for the refinements were all satisfactory, with R_{wp} in the range 3.7–4.7%. A plot of a selected range of the experimental data is presented in Fig. 6. Crystallographic and Rietveld refinement parameters for selected scans are presented in Table 1 and an example of Rietveld-type plot (data collected at $T = 92$ °C) is presented in Fig. 7, where similar abundances of γ- (34%) and α- (42%) are observed, with 17% of the initial alane already decomposed into Al.

Fig. 8 presents the obtained phase fractions and calculated hydrogen concentrations as a function of temperature while Figs. 9 and 10 show the evolution of the unit cell volumes and unit cell parameters for the two alane polymorphs as a function of the temperature. The γ-AlH_3 starts to decompose

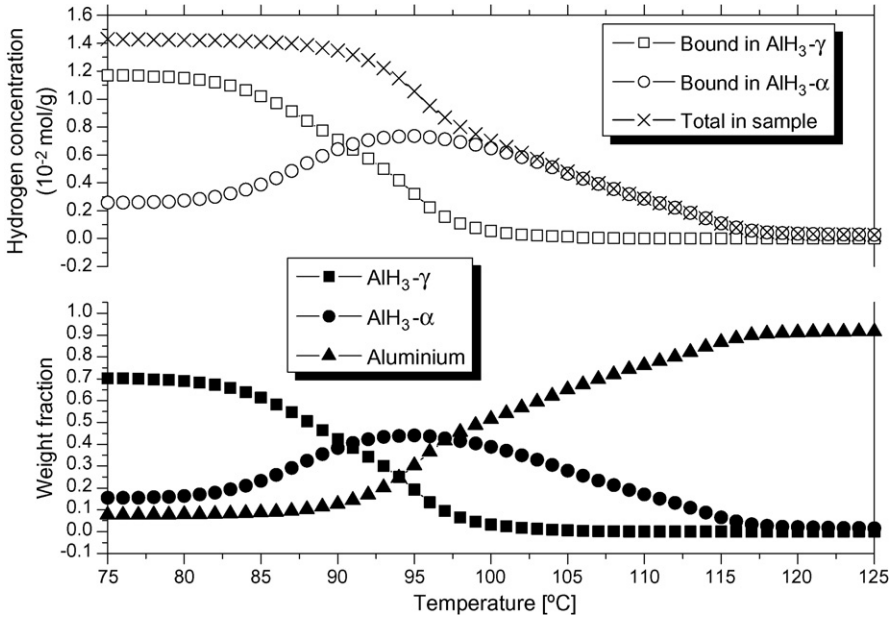

Fig. 8. Calculated phase percentages and hydrogen concentration from the *in situ* SR-XRD patterns of the γ-AlH_3 thermal decomposition.

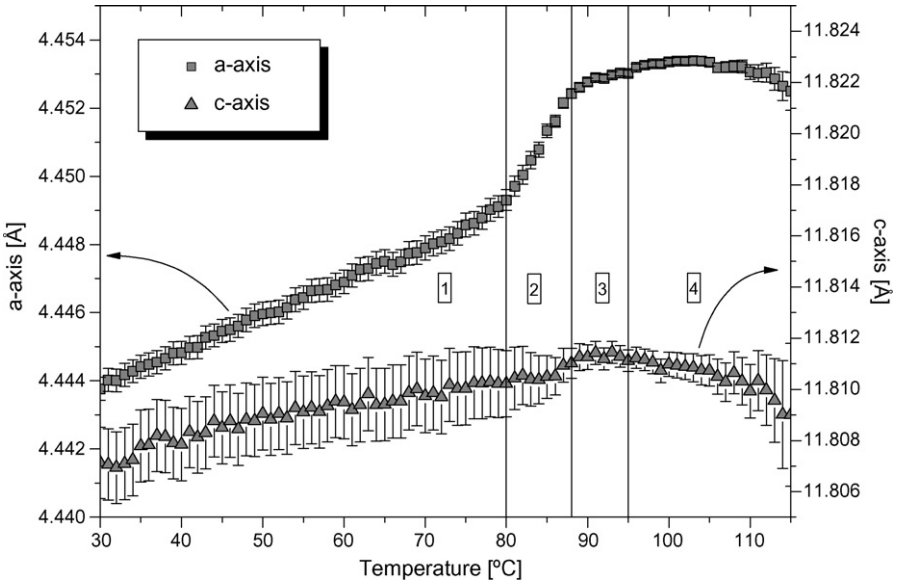

Fig. 9. Changes in unit cell dimensions for the α-AlH_3 phase *vs*. temperature from the *in situ* SR-XRD pattern of the γ-AlH_3 thermal decomposition. The numbers indicates the partition into temperature intervals with constant lattice changes: interval 1: (25–80 °C) constant phase fractions, mainly γ-AlH_3 present, 2: (80–88 °C) fast growth of α-AlH_3, growth of aluminium, γ-AlH_3 decreases, 3: (88–95 °C) slower growth of α-AlH_3, γ-AlH_3 decreases, fast growth of aluminium, 4: (95–115 °C) α-AlH_3 decreases to ∼0 at 115 °C, γ-AlH_3 decreases to ∼0 at 100 °C, steady growth of aluminium.

at $T \sim 80\,^{\circ}C$ and the content of aluminium and α-AlH_3 starts to increase. As this happens, the anisotropic expansion of the α-AlH_3 unit cell gets more pronounced, as can be seen from Fig. 9. The unit cell axes expand almost linearly within limited temperature regions. Relative changes per degree Celsius ($\Delta F/\Delta T$) were obtained by linear fits of the values obtained from the Rietveld-type refinements within four chosen temperature partitions and are presented in Table 2 and graphically for the α-modification in Fig. 11. In the first partition (25–80 °C) before the decomposition of γ-AlH_3 sets in, a change $\Delta F/\Delta T$ of $0.23 \times 10^{-2}\,^{\circ}C^{-1}$ is observed for the *a*-axis of α-AlH_3 while the *c*-axis is almost constant. In partition 2 (80–88 °C), during the fast growth-regime of α-AlH_3, $\Delta F/\Delta T$ for the *a*-axis increases almost four-fold to $0.89 \cdot 10^{-2}\,^{\circ}C^{-1}$. The maximum formation rate of α-AlH_3 appears at 88 °C, and after this, in partition 3 (88–95 °C), the axes expansion slows down to values similar as for the first partition. At higher temperatures (95–115 °C), partition 4, both the amount of α-AlH_3 and γ-AlH_3 decreases to ∼0 (at ∼115 and ∼100 °C, respectively) and a possible small nearly isotropic contraction of the α-AlH_3 unit cell is observed. Representative Rietveld-plots for the different temperature regions are presented in Figs. 7 and 12.

To get a more detailed view of how the phase transformations proceed, the changes of hydrogen concentrations in

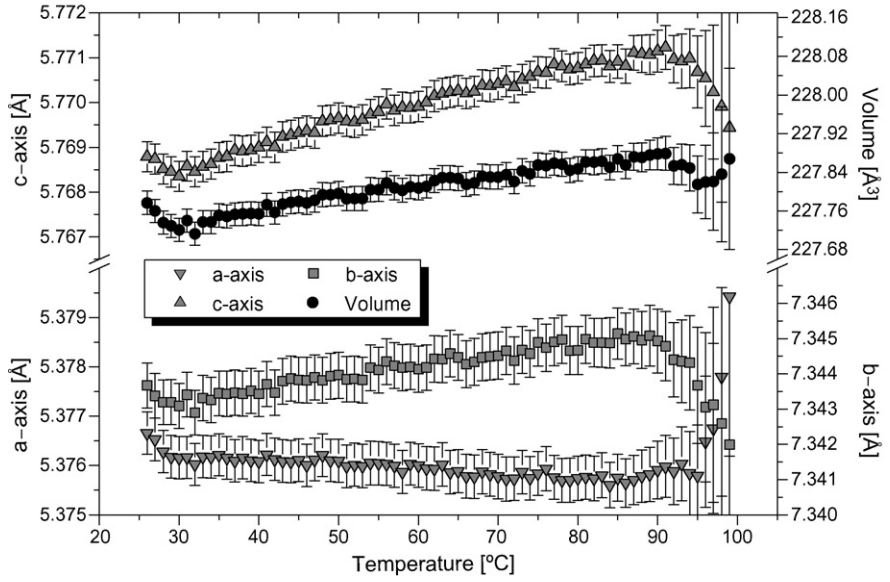

Fig. 10. Changes in unit cell dimensions for the γ-AlH_3 phase *vs*. temperature from the *in situ* SR-XRD patterns of the γ-AlH_3 thermal decomposition.

Table 2
Changes in lattice parameters as obtained from Rietveld-type fittings of *in situ* SR-XRD data of the thermal decomposition of AlH_3 samples

Phase	Variable (unit)	$T_{interval}$ (°C)	X_{start}[a]	X_{final}[a]	$\Delta F/\Delta T$[b] (10^{-2}%/°C)	Notes
α-AlH_3[c]	*a* (Å)	25–127.5	4.4567	4.4671	0.23	Only α-AlH_3 present AlH_3 (α-decomposition starts at ∼128 °C)
	c (Å)		11.8405	11.8392	−0.01	
	V (Å^3)		203.67	204.60	0.44	
α-AlH_3[d]	*a* (Å)	30–80	4.4438	4.4490	0.23	Mainly γ-phase present (constant phase fractions)
	c (Å)		11.8074	11.8105	0.05	
	V (Å^3)		201.93	202.46	0.52	
	a (Å)	80–88	4.4493	4.4525	0.89	γ-Phase starts to decompose, α-phase grows fast
	c (Å)		11.8103	11.8108	0.06	
	V (Å^3)		202.47	202.77	1.85	
	a (Å)	88–95	4.4525	4.4531	0.18	Slower α-phase growth (α formation peak ∼88 °C)
	c (Å)		11.8112	11.8113	0.01	
	V (Å^3)		202.79	202.84	0.38	
	a (Å)	95–115	4.4534	4.4529	−0.06	γ-Phase < 1 wt.% above 105 °C. α-phase decreases
	c (Å)		11.8114	11.8095	−0.08	
	V (Å^3)		202.87	202.79	−0.20	
γ-AlH_3[d]	*a* (Å)	30–75	5.37622	5.37579	−0.02	Mainly γ-phase present (constant phase fractions)
	b (Å)		7.34321	7.34474	0.05	
	c (Å)		5.76853	5.77069	0.08	
	V (Å^3)		227.73	227.85	0.11	

[a] Value of parameter obtained from linear fitting of lattice parameters in the range given in column '$T_{interval}$'. X_{start} is the first value in the temperature interval, X_{final}, the last. The lattice parameters used as data points in the fitting were obtained from Rietveld-type refinements of the experimental diffraction data.
[b] The fractional changes $\Delta F/\Delta T$ are defined as $100\cdot\Delta X/T$ where ΔX is $100\cdot(X_{final} - X_{start})/(X_{start})$.
[c] As obtained from the *in situ* SR-XRD study of thermal decomposition of 'aged' α-AlH_3.
[d] As obtained from the *in situ* SR-XRD study of thermal decomposition of γ-AlH_3.

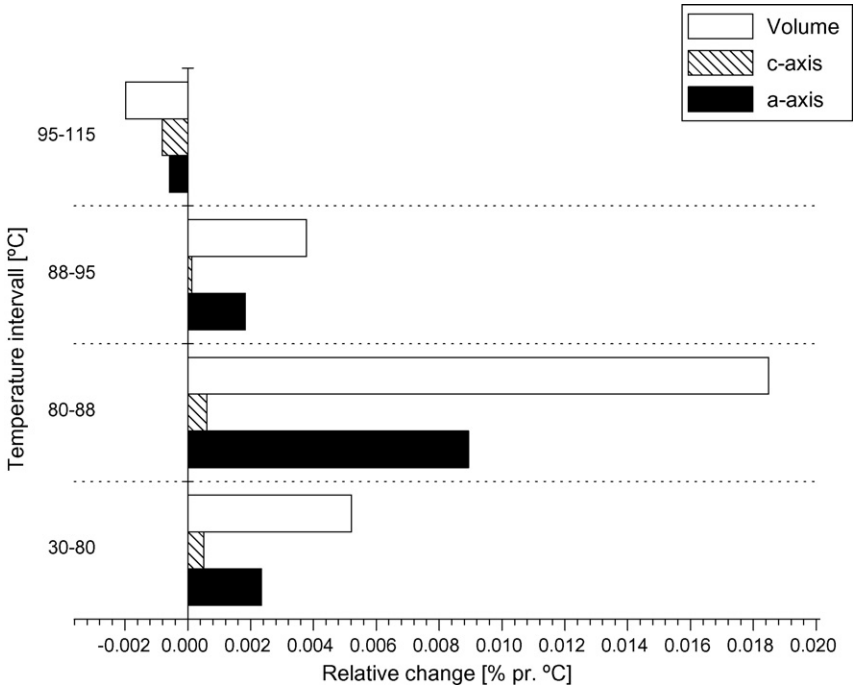

Fig. 11. Relative changes in unit cell dimensions for the α-AlH_3 phase *vs*. temperature from the *in situ* SR-XRD patterns of the γ-AlH_3 thermal decomposition.

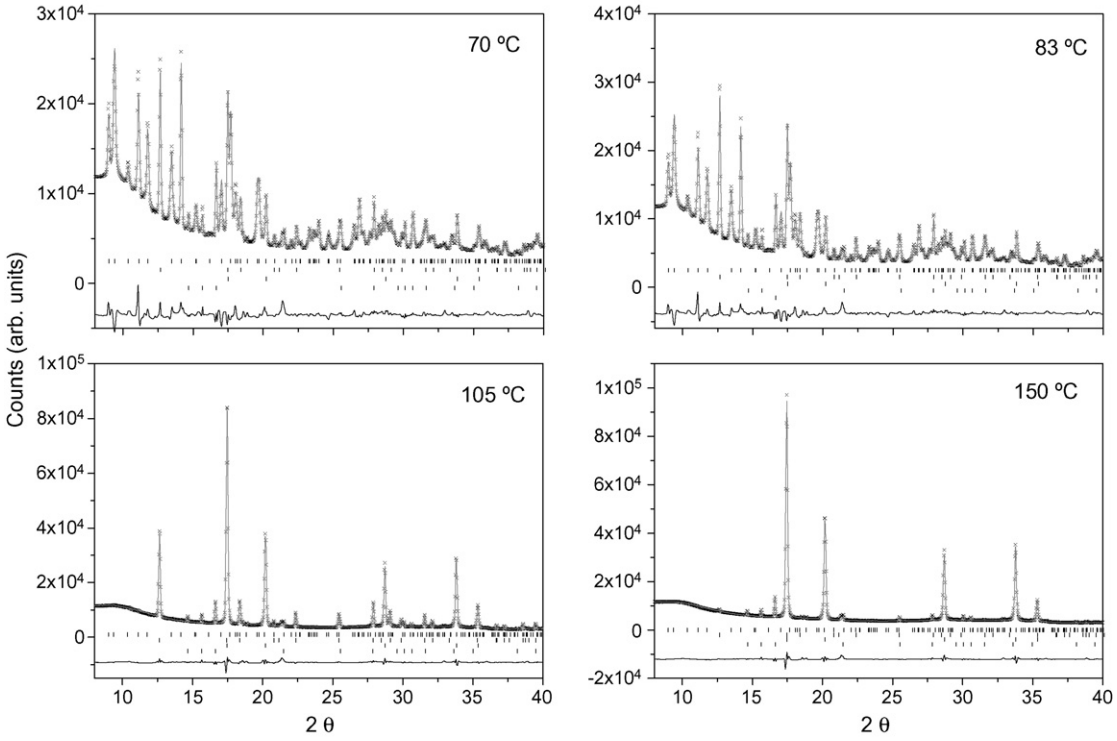

Fig. 12. Selected Rietveld-type plots of the *in situ* SR-XRD pattern of the γ-AlH_3 thermal decomposition showing observed (crosses), calculated (upper line) and difference (bottom line) plots. The positions of the Bragg peaks are shown as ticks (from top to bottom: γ-AlH_3, α-AlH_3, Al, impurity phases).

the hydride phases were calculated based on the weight fractions of the crystalline phases as obtained from the Rietveld refinements and assuming that hydrogen content decreases from 10 wt.% H to 0 during the decomposition process. The results are presented in Fig. 13 in the form of 'hydrogen desorption traces'. Formation of the α-phase consumes less hydrogen than the number of moles of hydrogen liberated by the decomposition of γ-AlH_3. Obviously, an excess of hydrogen is desorbed directly from the γ-AlH_3, *i.e.* due to direct transformation of γ-AlH_3 to aluminium. This provides an evidence of coexistence of two decomposition paths: γ-AlH_3 → Al, and γ-AlH_3 → α-AlH_3 → aluminium. From integrating the 'desorption traces', we arrive to a conclusion that direct decomposition of γ-AlH_3 is a prevailing process, yielding about 60% of the released hydrogen at the given heating rate (1/2 °C/min).

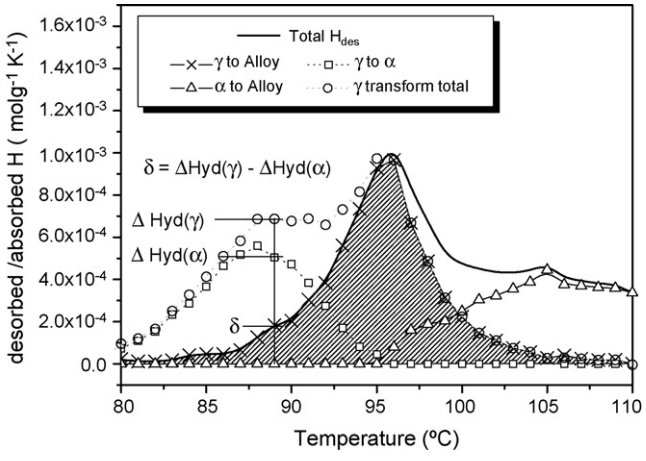

Fig. 13. Calculated hydrogen desorption and absorption traces from the *in situ* SR-XRD patterns of the γ-AlH_3 thermal decomposition. Subtracting the amount of hydrogen used during the formation of α-AlH_3 from the amount of hydrogen released by the decomposition of γ-AlH_3, a net hydrogen desorption trace is found (shaded area). This amount is attributed to direct γ-AlH_3 → Al phase transformation.

4. Summary

TDS studies and subsequent Arrhenius plots of fresh α-AlH_3 and γ-AlH_3 revealed that the activation energy of hydrogen desorption from γ-AlH_3, 92 kJ/mol AlH_3, is lower compared to α-AlH_3, 136 kJ/mol AlH_3. A TDS run of the aged α-AlH_3 sample showed a much higher desorption temperature compared to the freshly synthesized sample.

Crystal structure data for α-AlH_3, including the structure of hydrogen sublattice, was successfully obtained by Rietveld-type refinements and difference Fourier analysis of the high-resolution SR-XRD data. The refinements indicated a small charge transfer from Al to H atoms corresponding to the formation of $Al^{+0.15}$ and $H^{-0.05}$.

A significant anisotropic volume expansion of α-AlH_3 during its heating was observed with the main expansion proceeding along the *a*-axis and attributed to the elongations of the bridge bonds Al–H–Al aligned along [1 −1 1/2]. The expansion of the *a*-axis proceeds considerably faster during the fast "*in situ*" formation of the α-phase from the γ-hydride, as observed in the decomposition experiments of the γ-AlH_3. A small anisotropic expansion of the γ-AlH_3 was also observed.

In the decomposition experiment of the 'aged' α-AlH_3 sample, it seems that formation of an amorphous phase precedes the formation of aluminium and subsequently that the nucleation step limits the rate of aluminium formation. Aluminium forms easily in the γ-AlH_3 decomposition experiment. However, in this sample aluminium is already present of in the starting composition, providing already existing nuclei for the growth of aluminium. Thus, both experiments give complementary evidences that nucleation is the rate-limiting step in the growth of aluminium during the alane decomposition process. This observation agrees well with the findings of Graetz and Reilly [10].

From the analysis of the *in situ* SR-XRD pattern of the thermal decomposition of γ-AlH_3, evidence of two parallel decomposition processes of γ-hydride to aluminium were found (1) $\gamma \rightarrow Al$ and (2) $\gamma \rightarrow \alpha \rightarrow Al$. Direct decomposition process $\gamma \rightarrow Al$ was identified as a prevailing one.

Acknowledgements

This work received support from the Norwegian Research Council. We are grateful to Dr. M. Sato (Tokai University, Japan and IFE), T. Foerde (IFE) and Dr. A.B. Riabov (PhMI AS Ukraine) for their help.

References

[1] F.M. Brower, N.E. Matzek, P.F. Reigler, H.W. Rinn, C.B. Roberts, D.L. Schmidt, J.A. Snover, K. Terada, J. Am. Chem. Soc. 98 (1976) 2450–2453.
[2] A.E. Finholt, A.C. Bond, H.I. Schlesinger, J. Am. Chem. Soc. 69 (1947) 1199–1203.
[3] J.W. Turley, H.W. Rinn, Inorg. Chem. 8 (1969) 18.
[4] J.P. Maehlen, V.A. Yartys, in: D. Chandra, J. Petrovic, R.G. Bautista, A. Imam (Eds.), Symposium TMS 2006 Annual Meeting on Advanced Materials for Energy Conversion III, San Antonio, Texas, USA, March 12–16, 2006, pp. 77–85.
[5] V.A. Yartys, R.V. Denys, J.P. Maehlen, C. Frommen, M. Fichtner, B.M. Bulychev, H. Emerich, Inorg. Chem. 46 (2007) 1051–1055.
[6] H.W. Brinks, W. Langley, C.M. Jensen, J. Graetz, J.J. Reilly, B.C. Hauback, J. Alloys Compd., in press.
[7] S.-J. Hwang, R.C. Bowman, J. Graetz, J.J. Reilly, Mater. Res. Soc. Symp. Proc. 927 (2006), 0927-EE03-03 and S.-J. Hwang, R.C. Bowman, Jr., J. Graetz, J.J. Reilly, MH2006, O-071.
[8] G. Sandrock, J. Reilly, J. Graetz, W.M. Zhou, J. Johnson, J. Wegrzyn, Appl. Phys. A: Mater. Sci. Process. 80 (2005) 687–690.
[9] J. Graetz, J.J. Reilly, J. Alloys Compd. 424 (1/2) (2006) 262–265.
[10] J. Graetz, J.J. Reilly, J. Phys. Chem. B 109 (2005) 22181–22185.
[11] G. Sandrock, J. Reilly, J. Graetz, W.-M. Zhou, J. Johnson, J. Wegrzyn, J. Alloys Compd. 421 (1/2) (2006) 185–189.
[12] M. Stange, J.P. Maehlen, V.A. Yartys, P. Norby, W. van Beek, H. Emerich, J. Alloys Compd. 404 (2005) 604–608.
[13] P. Norby, J. Am. Chem. Soc. 119 (1997) 5215–5221.
[14] E.K. Andersen, I.G.K. Andersen, P. Norby, J.C. Hanson, J. Solid State Chem. 141 (1998) 235–240.
[15] H.M. Rietveld, J. Appl. Crystallogr. 2 (1969) 65–71.
[16] A.C. Larson, R.B.v. Dreele (LANL, Los Alamos, 1994).
[17] P. Thompson, D.E. Cox, J.B. Hastings, J. Appl. Crystallogr. 20 (1987) 79–83.
[18] C.J. Howard, J. Appl. Crystallogr. 15 (1982) 615–620.
[19] L.W. Finger, D.E. Cox, A.P. Jephcoat, J. Appl. Crystallogr. 27 (1994) 892–900.
[20] P.W. Stephens, J. Appl. Crystallogr. 32 (1999) 281–289.
[21] V.A. Yartys, V.V. Burnasheva, K.N. Semenenko, Usp. Khim. 52 (1983) 529–562.
[22] V.A. Yartys, V.V. Burnasheva, K.N. Semenenko, N.V. Fadeeva, S.P. Solovev, Int. J. Hydrogen Energy 7 (1982) 957–965.